Direct inhibition of oncogenic KRAS by hydrocarbon-stapled SOS1 helices

Elizaveta S. Leshchiner[a], Andrey Parkhitko[b], Gregory H. Bird[a], James Luccarelli[a], Joseph A. Bellairs[a], Silvia Escudero[a], Kwadwo Opoku-Nsiah[a], Marina Godes[a], Norbert Perrimon[b,c], and Loren D. Walensky[a,1]

[a]Department of Pediatric Oncology and the Linde Program in Cancer Chemical Biology, Dana–Farber Cancer Institute, Boston, MA 02215; and [b]Department of Genetics and [c]Howard Hughes Medical Institute, Harvard Medical School, Boston, MA 02115

Edited by James A. Wells, University of California, San Francisco, CA, and approved December 31, 2014 (received for review July 11, 2014)

Activating mutations in the Kirsten rat sarcoma viral oncogene homolog (KRAS) underlie the pathogenesis and chemoresistance of ∼30% of all human tumors, yet the development of high-affinity inhibitors that target the broad range of KRAS mutants remains a formidable challenge. Here, we report the development and validation of stabilized alpha helices of son of sevenless 1 (SAH-SOS1) as prototype therapeutics that directly inhibit wild-type and mutant forms of KRAS. SAH-SOS1 peptides bound in a sequence-specific manner to KRAS and its mutants, and dose-responsively blocked nucleotide association. Importantly, this functional binding activity correlated with SAH-SOS1 cytotoxicity in cancer cells expressing wild-type or mutant forms of KRAS. The mechanism of action of SAH-SOS1 peptides was demonstrated by sequence-specific down-regulation of the ERK-MAP kinase phosphosignaling cascade in KRAS-driven cancer cells and in a *Drosophila melanogaster* model of *Ras85D*^{V12} activation. These studies provide evidence for the potential utility of SAH-SOS1 peptides in neutralizing oncogenic KRAS in human cancer.

RAS | inhibitor | SOS1 | stapled peptide | cancer

RAS signaling is a critical control point for a host of cellular functions ranging from cellular survival and proliferation to cellular endocytosis and motility (1). The on or off state of RAS is dictated by nucleotide exchange. GTP-bound RAS is the activated form that engages its downstream effectors with high avidity. The endogenous GTPase activity of RAS hydrolyzes GTP to GDP and inactivates signaling. This biochemical process is further regulated by GTPase-activating proteins (GAPs) that impair RAS signaling through increasing endogenous GTPase activity and guanine-nucleotide exchange factors (GEFs) that enhance RAS signaling by facilitating GDP release and, thus, GTP association. Given the central roles of RAS in cellular growth and metabolism, it is not surprising that cancer cells usurp its prosurvival activities to achieve immortality.

Activating mutations in KRAS represent the most frequent oncogenic driving force among the RAS homologs K-, N-, and H-RAS, and are associated with poor prognosis and chemoresistance (2). KRAS mutations are present in ∼30% of human tumors and at even higher frequencies in cancers of the pancreas, lung, thyroid gland, colon, and liver. For example, in pancreatic ductal adenocarcinomas (PDAC) that carry a 5-y survival rate of less than 5%, activating KRAS mutations are present in more than 90% of tumors (3). Thus, therapeutic inhibition of RAS is among the highest priority goals of the cancer field. Because oncogenic forms of KRAS typically harbor single-point mutants that stabilize its active GTP-bound form, a host of recent small molecule and peptide development efforts have been aimed at disarming this pathologic biochemical state. The extremely high affinity of KRAS for its GTP substrate has hampered the development of competitive GTP inhibitors. However, a GDP mimetic that covalently modifies the mutant cysteine of KRAS G12C represents a promising approach to plugging the nucleotide-binding site (4). The prototype compound SML-10-70-1 demonstrated antiproliferative effects in the 25–50 μM range, although it did not appear to discriminate between KRAS-dependent and KRAS-independent growth (4). An elegant screening strategy based on covalent engagement of the G12C thiol identified promising inhibitors that target a new allosteric site adjacent to the nucleotide exchange region (5). These compounds not only switched the nucleotide-binding preference of KRAS G12C to GDP over GTP (5), favoring the inactive state, but may also diminish effector interactions, a distinct and complementary RAS-inhibitory activity exploited by another series of small molecules recently identified by in silico screening (6). Compounds that emerged from these molecular tethering and in silico strategies have demonstrated micromolar and submicromolar range antitumor responses in cancer cells driven by KRAS G12C and KRAS G12V, respectively (5, 6).

Because the KRAS-GDP to KRAS-GTP transition catalyzed by the GEF, son of sevenless 1 (SOS1), represents the rate-limiting step for nucleotide exchange (7, 8), disrupting the activating SOS1/KRAS protein interaction has also been the focus of drug development efforts (9). A synthetic peptide incorporating select residues of the SOS1 helical interaction motif and structurally stabilized by hydrogen bond surrogate (HBS) chemistry yielded mid- to high-micromolar binders that inhibited wild-type Ras-ERK phosphosignaling (10). Two NMR-based fragment screens independently identified small molecules that also bind to KRAS in the mid- to high-micromolar range and disrupted SOS1-mediated RAS activation (11, 12). However, the effects of these new peptidic and small molecule agents on cancer cell viability were not evaluated (10–12). In an interesting twist, a set of recently

Significance

KRAS is one of the most prevalent and vicious oncogenic proteins, yet no drugs are available to inhibit its pathologic activity in patients. We report that KRAS-targeting stapled peptides, modeled after the native son of sevenless 1 (SOS1) helical domain, engage wild-type and clinically relevant KRAS mutant proteins with nanomolar affinity. To our knowledge, these compounds represent the highest affinity and broadest spectrum binders of KRAS mutants reported to date. The stapled peptides disrupt the SOS1/KRAS protein interaction and directly inhibit nucleotide association to wild-type and mutant KRAS proteins. We correlate functional binding activity with SAH-SOS1 cytotoxicity across a 13-member panel of KRAS-driven cancer cells and demonstrate sequence- and dose-dependent inhibition of the ERK-MAP kinase phosphosignaling cascade downstream of KRAS in vitro and in vivo.

Author contributions: E.S.L., A.P., G.H.B., J.L., N.P., and L.D.W. designed research; E.S.L., A.P., G.H.B., J.L., J.A.B., S.E., K.O.-N., M.G., N.P., and L.D.W. performed research; E.S.L., A.P., G.H.B., N.P., and L.D.W. contributed new reagents/analytic tools; E.S.L., A.P., G.H.B., J.L., J.A.B., K.O.-N., N.P., and L.D.W. analyzed data; and E.S.L., N.P., and L.D.W. wrote the paper.

Conflict of interest statement: L.D.W. is a scientific advisory board member and consultant for Aileron Therapeutics.

This article is a PNAS Direct Submission.

[1]To whom correspondence should be addressed. Email: loren_walensky@dfci.harvard.edu.

This article contains supporting information online at www.pnas.org/lookup/suppl/doi:10.1073/pnas.1413185112/-/DCSupplemental.

described small molecule hits engaged the RAS–SOS1–RAS ternary complex at a unique hydrophobic pocket, activated nucleotide exchange, and perturbed phosphosignaling downstream of RAS (13). Finally, a combinatorial screening approach identified several cyclic peptides with submicromolar RAS-binding activity, but no cellular activity was observed (14). Despite the recent progress in developing small molecules and synthetic peptides to directly target RAS or RAS-SOS1, high-affinity binders with promising cellular activity across the broad spectrum of wild-type and mutant KRAS-driven cancers have remained out of reach. Thus, there is a pressing need for next-generation agents to target and disarm KRAS in human cancer cells.

We have previously generated "stapled peptides" modeled after key α-helical interaction domains to disrupt oncogenic protein interactions of the BCL-2 family, p53, β-catenin, and EZH2 pathways (15–18). By sampling alternative staple positions, interrogating cellular uptake, and correlating biochemical function with antitumor activity and mechanism of action, we have generated lead compounds that form the basis for therapeutic development (16, 17, 19, 20). Here, we report the application of all-hydrocarbon stapling to recapitulate the native primary sequence and secondary structure of the RAS-interacting α-helix of SOS1. Our goal was to develop a direct inhibitor that binds the diversity of KRAS mutant forms, impairs nucleotide exchange and, importantly, broadly kills KRAS-mutant cancer cells in a sequence-specific manner by deactivating its downstream phosphosignaling cascade.

Results

SAH-SOS1 Peptides Bind to Wild-Type and Mutant KRAS with Nanomolar Affinity. The crystal structure of the complex between the SOS1 catalytic domain and KRAS (PDB ID code: 1NVU) (21) demonstrated direct contact between a SOS1 α-helix (cyan) and KRAS, implicating this interface in catalyzing nucleotide exchange (Fig. 1*A*). Using the primary sequence of this SOS1 α-helix (amino acids 929–944), we generated a series of stabilized alpha helices of SOS1 (SAH-SOS1) peptides bearing alternatively positioned i, i+4 staples (Fig. 1*A* and Fig. S1*A*). The resultant SAH-SOS1 a–d peptides were then screened by fluorescence polarization (FP) assay for binding activity to recombinant hexahistidine-tagged (His_6) KRAS proteins, including wild-type and G12D, G12V, G12C, G12S, and Q61H mutant forms (Fig. S1*B*). Whereas SAH-SOS1 peptides a, c, and d demonstrated nanomolar binding activity in the 60–160 nM range, SAH-$SOS1_b$ showed little to no interaction, consistent with the disruptive location of its staple at the KRAS binding interface (Fig. 1*A* and Fig. S1).

We selected SAH-$SOS1_a$ for further development based on its superior binding activity and solubility profile, and also advanced SAH-$SOS1_b$ as an ideal negative control for biochemical and cellular studies. To optimize these constructs for cellular work, we further appended two Arg residues at the N termini to adjust the overall charge of the peptides from −1 to +1, based on our longstanding observation across multiple stapled peptide templates that cellular uptake is enhanced when overall charge is ≥0 (22, 23). We confirmed the cellular penetrance of these revised constructs (Table S1 and Fig. S2), hereafter referred to as SAH-$SOS1_A$ and SAH-$SOS1_B$ (using capital letter subscripts), by confocal microscopy (Fig. S3*A*), fluorescence scan of electrophoresed lysates from treated cells (Fig. S3*B*), and high-content microscopic imaging analysis (Fig. S4). We then repeated the FP binding analyses by using our positive and negative control SAH-SOS1 constructs, documenting a 100- to 175-nM binding range for SAH-$SOS1_A$ across the His_6-KRAS proteins, with no binding activity observed for SAH-$SOS1_B$ (Fig. 1). As an additional measure of relative binding activity, we demonstrated that SAH-$SOS1_A$, but not SAH-$SOS1_B$, disrupted the protein interaction between recombinant GST-KRAS and His_6-SOS1 proteins in vitro (Fig. S5*A*). We confirmed that SAH-$SOS1_A$ was capable of dissociating the protein complex owing to its capacity to directly target KRAS in solution, as demonstrated by streptavidin pull-down of biotinylated SAH-$SOS1_A$ and anti-KRAS Western blot analysis (Fig. S5*B*). Thus, we find that insertion of an all-hydrocarbon staple into the native SOS1 sequence (amino acids 929–944) at the noninteracting helical face yields peptidic ligands that bind to KRAS in the nanomolar range, representing at least a two orders of magnitude improvement over the recently published peptide and small molecule inhibitors of the KRAS/SOS1 interface.

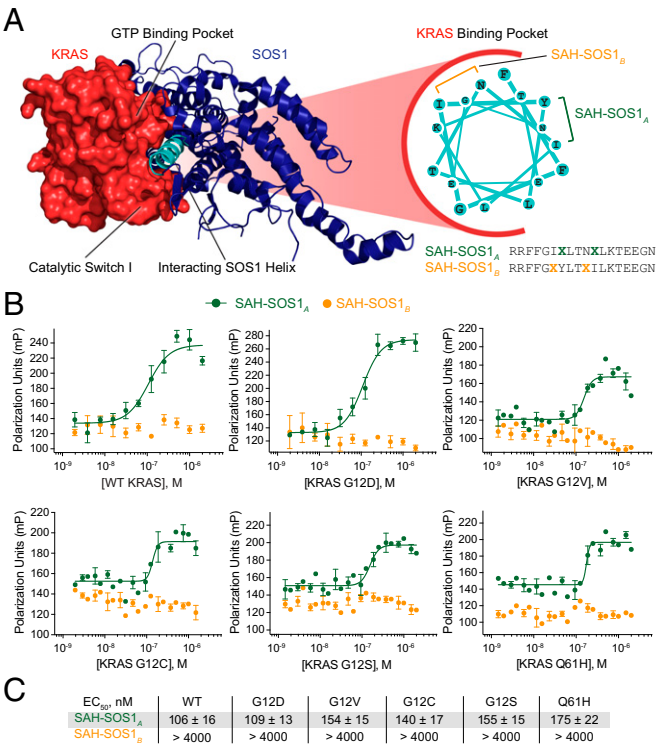

Fig. 1. Design and KRAS binding activity of SAH-SOS1 peptides. (*A*) The crystal structure of KRAS (red) in complex with its guanidine exchange factor SOS1 (blue) revealed a binding interaction between the indicated SOS1 α-helix (cyan) and KRAS (PDB ID code 1NVU). SAH-SOS1 peptides were generated by inserting all-hydrocarbon staples at positions A (green) and B (orange) into a SOS1 peptide spanning amino acids 929–944 and bearing an N-terminal Arg-Arg tag to optimize cellular penetrance. (*B*) Fluorescence polarization binding analysis of FITC-labeled SAH-SOS1 peptides and recombinant KRAS proteins, including wild-type and mutant variants. Data are mean ± SEM for experiments performed in technical triplicate and are representative of at least three biological replicates performed with independent preparations of recombinant KRAS proteins. (*C*) Table of EC_{50} values for the binding interactions between SAH-SOS1 peptides and the individual KRAS proteins.

SAH-$SOS1_A$ Engages both GDP-KRAS and GTP-KRAS. Because KRAS exists in two distinct conformations depending on its interaction with GDP vs. GTP (24), we next tested whether SAH-$SOS1_A$ engages one or both forms of KRAS. FP analysis using GDP- and GTP-loaded, recombinant, wild-type KRAS revealed equivalent SAH-$SOS1_A$ binding affinities (Fig. S6*A*), consistent with the capacity of SAH-$SOS1_A$ to engage both forms of KRAS. As an additional measure of direct binding activity, we performed differential scanning fluorimetry by using GDP- and GTP-loaded forms of KRAS in the presence or absence of SAH-$SOS1_A$ or the negative control peptide SAH-$SOS1_B$. GTP-loaded KRAS demonstrated a lower melting temperature than GDP-loaded KRAS (Fig. S6*B*), reflecting the more rigid structure of the GDP-loaded form (and relative inaccessibility of the SYPRO dye until the GDP-loaded form unfolds at the higher temperature). Upon addition of SAH-$SOS1_A$, both forms of KRAS demonstrate a shift in the melting curve, consistent with a small increase in conformational flexibility from ligand binding. Indeed, the SOS1 interaction is believed to favor the KRAS "open" conformation (21), and allosteric release of nucleotide can also decrease the structural

stability of the KRAS protein (25). Importantly, the observed changes in KRAS are peptide sequence-specific, as the negative control stapled peptide, SAH-SOS1$_B$, had no such effect (Fig. S6*B*).

To further confirm that SAH-SOS1$_A$ peptide specifically targets KRAS at the SOS1 binding pocket, we performed NMR analysis of GDP-loaded ^{15}N-KRAS upon incubation with SAH-SOS1$_A$. We find that the overall fold of KRAS is preserved upon SAH-SOS1$_A$ engagement, and discrete chemical shift changes occur in residues that colocalize at the SOS1-binding site (see below) and the very region of KRAS implicated in conformational opening during SOS1 protein engagement (e.g., H27, F28, V29, R149) (Fig. 2 *A* and *B*). A calculated model structure derived from docking analyses demonstrated the juxtaposition of SAH-SOS1$_A$ residues with the majority of residues that undergo chemical shift change, such as L6, G15, L56, D57, E63, Y64, R73, T74, and Q99 (Fig. 2*C*). Taken together, our biochemical data demonstrate that SAH-SOS1$_A$ directly binds to both GDP- and GTP-loaded forms of KRAS, with the structural analysis implicating the SOS1-binding pocket as the functional site of SAH–SOS1$_A$ interaction.

SAH-SOS1$_A$ Directly Inhibits Nucleotide Association to KRAS. We next sought to determine whether the direct binding of SAH-SOS1$_A$ could independently impact the capacity of KRAS to exchange nucleotide and, in particular, the activating nucleotide association process. The addition of the fluorescent GTP analog, mant-GTP (2′-/3′-*O*-(*N*′-methylanthraniloyl)guanosine-5′-*O*-triphosphate), associated with wild-type His$_6$-KRAS in a time-dependent fashion, as demonstrated by the increase in measured fluorescence (Fig. 3*A*). As a negative control, we incubated KRAS with mant-GTP and excess unlabeled GTP, which completely blocked mant-GTP association (Fig. 3*A*). We then coincubated KRAS with mant-GTP and either SAH-SOS1$_A$ or SAH-SOS1$_B$. Whereas SAH-SOS1$_A$ dose-responsively inhibited mant-GTP association, SAH-SOS1$_B$ had little to no effect (Fig. 3*A*).

To evaluate the functional impact of SAH-SOS1 peptides on the G12D mutant form of KRAS, mant-GDP association was examined because of the slower kinetics of mant-GTP binding in this experimental context. The incubation of His$_6$-KRAS G12D with mant-GDP resulted in time-responsive association, which was blocked upon coincubation with excess unlabeled GDP (Fig. 3*B*). As above, coincubation of KRAS G12D with mant-GDP and SAH-SOS1$_A$ peptide dose-responsively blocked nucleotide association, whereas SAH-SOS1$_B$, which does not bind to wild-type or mutant KRAS, had no effect. Thus, we find that engagement of wild-type or KRAS G12D by SAH-SOS1$_A$ independently blocks the capacity of KRAS to engage nucleotides in both a dose-responsive and sequence-dependent fashion.

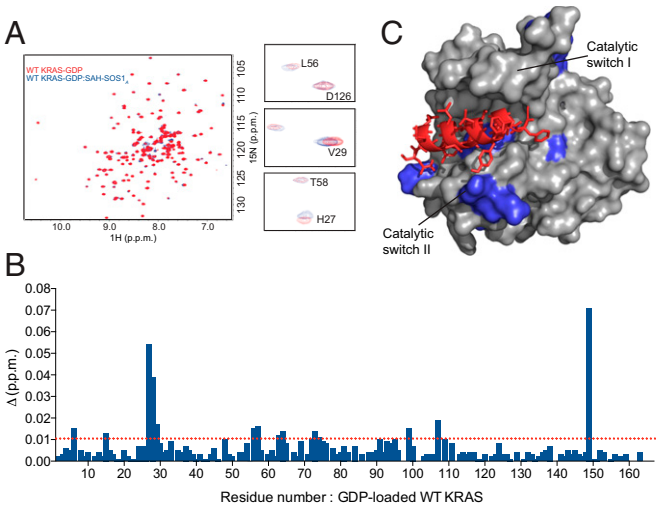

Fig. 2. NMR analysis of SAH-SOS1$_A$/KRAS interaction. (*A*) ^{1}H-^{15}N HSQC spectrum of uniformly ^{15}N-labeled GDP-loaded WT KRAS in the absence (red) or presence of SAH-SOS1$_A$ (blue). (*B*) Chemical shift changes (significance threshold > 0.01 ppm) are plotted as a function of WT KRAS residue number. (*C*) SAH-SOS1$_A$ was docked onto KRAS (starting structural model PDB ID code 1NVU; HADDOCK software) based on HSQC data. The calculated model structure depicts the SOS1 helix engaging the SOS1-binding pocket of KRAS.

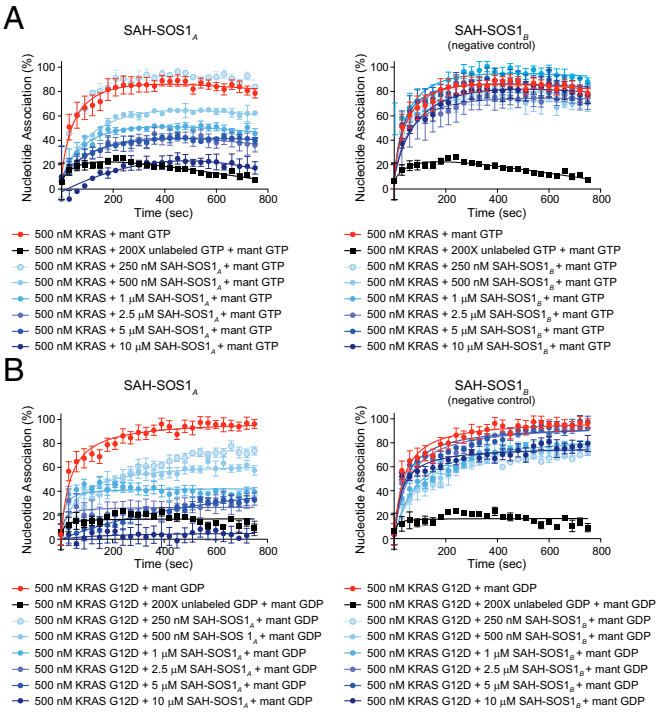

Fig. 3. SAH-SOS1$_A$ inhibits nucleotide association with wild-type and mutant KRAS. (*A* and *B*) The indicated fluorescent nucleotide analogs were incubated with wild-type (*A*) or G12D mutant (*B*) KRAS protein and the increase in fluorescence was monitored over time (red). Coincubation with unlabeled nucleotide served as a negative control (black). A serial dilution of SAH-SOS1 peptides were coincubated with KRAS and fluorescent nucleotide at the indicated doses to monitor for effects on nucleotide association. Data are mean ± SEM for experiments performed in at least technical triplicates and are representative of two biological replicates performed with independent preparations of recombinant KRAS proteins.

SAH-SOS1$_A$ Impairs the Viability of KRAS-Mutant Cancer Cells. Whereas micromolar quantities of small molecules and peptides were shown to target the SOS1/KRAS binding region and disrupt nucleotide exchange activity (10–12), the effect of these agents on cancer cell viability was not explored. We therefore tested whether our lead SAH-SOS1$_A$ construct, which binds to wild-type and mutant forms of KRAS in the 100- to 175-nM range, could inhibit the viability of pancreatic, colon, and lung cancer cells bearing distinct KRAS mutations. We found that SAH-SOS1$_A$, but not the negative control peptide SAH-SOS1$_B$, dose-responsively impaired the viability of cancer cells bearing KRAS G12D (Fig. 4*A* and Fig. S7*A*), G12C (Fig. S7*B*), G12V (Fig. S7*C*), G12S (Fig. S7*D*), G13D (Fig. S7*E*), and Q61H (Fig. S7*F*) mutations with IC$_{50}$ values in the 5- to 15-μM range. Cancer cells expressing wild-type KRAS, such as HeLa and Colo320-HSR cells, were similarly affected (Fig. S8*A*). Importantly, we confirmed that at the doses that SAH-SOS1$_A$ was cytotoxic to cells, the stapled peptide was soluble and monomeric (Fig. S9).

To further probe the specificity of SAH-SOS1$_A$ activity, we generated five mutant constructs that incorporated, for example, conversions of select hydrophobic residues to charged residues, and hydrophilic residues to hydrophobic residues (Fig. 4*B*). We then measured His$_6$-KRAS G12D binding activity and cell viability responses in the KRAS G12D-bearing Panc 10.05 cancer

BIOCHEMISTRY

line. Strikingly, those SAH-SOS1$_A$ mutant peptides that retained KRAS G12D binding activity (mut1–2) inhibited cell viability, whereas those mutants that lost binding activity (mut3–5) had no effect on cancer cell viability (Fig. 4 *C* and *D*). Thus, we find that SAH-SOS1$_A$ manifests dose-responsive and sequence-specific antitumor activity across a broad spectrum of wild-type and mutant KRAS-expressing cancer cell lines.

SAH-SOS1$_A$ Inhibits Phosphosignaling Downstream of KRAS in Vitro and in Vivo. To determine whether the observed inhibitory effect of SAH-SOS1$_A$ on cancer cell viability could be linked to negative modulation of KRAS signaling activity, we examined the dose-dependent effects of SAH-SOS1$_A$ treatment on the phosphorylation state of MEK, ERK, and AKT in Panc 10.05 cells exposed to EGF. Whereas SAH-SOS1$_A$ dose-responsively inhibited MEK1/2, ERK1/2, and AKT phosphorylation, SAH-SOS1$_B$ had no effect (Fig. 5*A*). An analogous SAH-SOS1$_A$-specific effect was observed in HeLa cells bearing wild-type KRAS (Fig. S8*B*). Importantly, the dosing at which SAH-SOS1$_A$ down-regulated phosphorylation matched the concentrations required to impair cancer cell viability (Figs. 4*A* and 5*A* and Fig. S8).

Finally, we evaluated whether the inhibitory effects of SAH-SOS1$_A$ on KRAS signaling observed in cancer cells could be extended to an in vivo context. For this work, we used an inducible system in *Drosophila melanogaster* for Ras1, the major *Drosophila* homolog of N-ras, H-ras, and K-ras genes (26). In this model, Actin Geneswitch (ActinGS) drives broad and high level tissue expression of a V12-mutant form of RAS85D upon treatment with RU486 (27). For our first study, we induced RAS85D^{V12} for

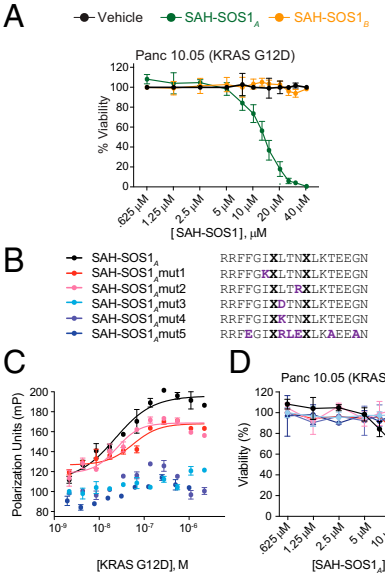

Fig. 4. SAH-SOS1$_A$ cytotoxicity correlates with KRAS binding activity. (*A*) SAH-SOS1$_A$, but not SAH-SOS1$_B$, dose-responsively inhibits the viability of Panc 10.05 cells bearing the KRAS G12D mutation. Cells were treated with vehicle, SAH-SOS1$_A$, or SAH-SOS1$_B$, and cell viability was measured at 24 h by CellTiterGlo assay. Data are mean ± SEM for experiments performed in at least duplicate and representative of at least two biological replicates performed with independent cancer cell cultures. (*B*) A panel of SAH-SOS1$_A$ mutant peptides was generated for structure activity relationship studies. (*C*) Fluorescence polarization binding analysis of SAH-SOS1$_A$ peptides and recombinant KRAS G12D protein. Data are mean ± SEM for experiments performed in technical duplicate and representative of at least three biological replicates performed with independent preparations of recombinant KRAS protein. (*D*) Panc 10.05 cells were treated with the panel of SAH-SOS1$_A$ peptides and cell viability measured at 24 h by CellTiterGlo assay. Data are mean ± SEM for experiments performed in at least technical duplicates and are representative of at least two biological replicates performed with independent cancer cell cultures.

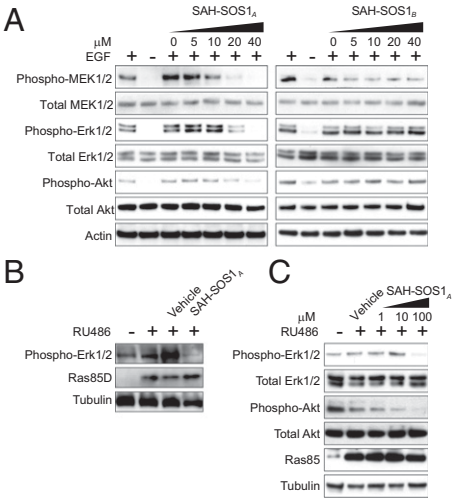

Fig. 5. SAH-SOS1$_A$ inhibits phosphosignaling downstream of KRAS in vitro and in vivo. (*A*) Panc 10.05 cells were incubated with vehicle, SAH-SOS1$_A$, or SAH-SOS1$_B$ at the indicated doses for 4 h, followed by 15-min stimulation with EGF. Cellular lysates were then electrophoresed and subjected to Western blot analysis by using antibodies to phospho- and total MEK1/2, ERK1/2, and Akt. (*B*) Vehicle (DMSO) or SAH-SOS1$_A$ (0.2 μL of 10 mM solution) was injected into the abdomens of *D. melanogaster* Ras85D^{V12}/ActinGS ($n = 5$ per arm) after a 3-d period of RAS induction by RU486 treatment (150 μg/mL in 2 mL of fly food). Flies were collected 48 h after SAH-SOS1$_A$ peptide injection, and lysates were processed for electrophoresis and Western blot analysis by using anti-phospho-ERK1/2 antibody. (*C*) *D. melanogaster* Ras85D^{V12}/ActinGS ($n = 20$ per arm) treated with vehicle or RU486 (150 μg/mL) alone, or cotreated with RU486 and SAH-SOS1$_A$ (1, 10, or 100 μM in 2 mL of fly food). After 4 d of oral treatment, tissue lysates were subjected to electrophoresis and Western blotting for phospho- and total ERK1/2 and Akt.

3 d by using 150 μM RU486, which was added directly to the fly food. We then injected vehicle or SAH-SOS1$_A$ directly into the fly abdomens, and 48 h later performed Western blotting for phospho-ERK1/2 on the harvested tissue extracts. SAH-SOS1$_A$ treatment notably decreased the phosphorylation state of ERK1/2 (Fig. 5*B*). Next, we added SAH-SOS1$_A$ directly to the fly food, as for RU486, and after 3 d of RAS85D^{V12} induction, Western blotting for phospho-ERK1/2 and phospho-AKT was performed. We observed near complete suppression of ERK1/2 and AKT phosphorylation at the 100 μM SAH-SOS1$_A$ dosing level (Fig. 5*C*). To probe the specificity of the response, we repeated the experiment comparing responses to vehicle, SAH-SOS1$_A$, and SAH-SOS1$_B$ after 3 and 5 d treatment with RU486 and SAH-SOS1 peptides. In each case, we observed a decrease in ERK1/2 phosphorylation upon SAH-SOS1$_A$ treatment, whereas SAH-SOS1$_B$ had no effect (Fig. S10). Of note, SAH-SOS1 peptides had no independent effect on the levels of RAS or ERK protein, and no fly toxicity was observed from the treatments.

Discussion

KRAS is one of the most pervasive pathogenic factors in human cancer but no drugs are available for clinical use to directly bind and block this deadly protein. Over the last few years, there has been a flurry of new reports suggesting that small molecules and peptide prototypes may, in fact, be capable of engaging KRAS to block its GTP binding site, impair nucleotide exchange, tip the equilibrium in favor of the inactive state, and/or block interactions with effectors. Whereas the majority of approaches have achieved proof-of-concept for engagement of RAS or KRAS, and consequent biochemical modulation (albeit at mid- to high-micromolar concentrations), anticancer activity was either not yet explored, not observed, or required dosing levels that would preclude clinical translation. A notable exception are compounds that engage a novel binding pocket beneath the effector binding

switch-II region of the G12C mutant form of KRAS. These new agents exhibited submicromolar antiproliferative activity specifically in KRAS G12C-driven cancer cells. Indeed, all of these new strategies hold promise that further iteration and optimization could lead to a breakthrough anti-KRAS agent. In the meantime, continued exploration of chemical space and extension of structural and biochemical studies into the cellular and in vivo realms is required.

Stapled peptides are a relatively new class of structured peptides, designed to mimic bioactive helices yet remedy the traditional shortcomings of peptide therapeutics, namely loss of shape, proteolytic lability, and difficulty accessing intracellular targets. When appropriately designed and optimized, stapled peptides can manifest remarkable structural stability, extracellular and intracellular protease resistance, and the capacity to gain entry to the cell via energy-dependent macropinocytosis (18, 23). Sampling a series of staple locations along the length of the peptide can yield high-affinity binders and, importantly, negative control compounds based on the replacement of key amino acid residues or steric interference of the staple at the binding interface. Here, we find that SAH-SOS1$_A$ can target the SOS1-binding pocket on KRAS with nanomolar affinity, directly and independently block nucleotide association, impair KRAS-driven cancer cell viability, and exert its effects by on-mechanism blockade of the phosphosignaling cascade downstream of KRAS. Importantly, all of these activities are dose- and sequence-dependent. Using a *Drosophila* model of induced mutant RAS expression, we find that the effects of SAH-SOS1$_A$, administered by injection or orally, extend to an in vivo context. Thus, a peptide-stapling approach to targeting the SOS1 regulatory groove on KRAS may be a viable strategy for therapeutic development.

One of the most promising features of our stapled peptide results is the broad spectrum, nanomolar targeting capacity of SAH-SOS1$_A$ across both wild-type and a diversity of KRAS mutant forms. Indeed, SAH-SOS1 peptides are among the highest affinity KRAS binders reported to date, and address the most clinically relevant forms of mutant KRAS, including the G12V, G12D, G12C, G12S, G13D, and Q61H variants. Importantly, the SAH-SOS1$_A$ approach can harness dual biochemical activities, in that it can both disrupt the activating SOS1/KRAS protein interaction, while also independently block nucleotide association as a direct result of its interaction with KRAS. It appears that the SOS1-binding interface provides a platform for SAH-SOS1$_A$ engagement of KRAS irrespective of mutant form, with peptide interaction effectively and uniformly blocking nucleotide association, as exemplified by our biochemical results using recombinant wild-type and G12D-mutant KRAS. Indeed, more than a dozen cancer lines expressing either wild-type or mutant KRAS protein were susceptible to SAH-SOS1$_A$ treatment.

A potential therapeutic window for this treatment strategy may derive from the relative dependency of such cancer cells on KRAS compared with normal cells. Our studies in *Drosophila* did not reveal toxicity from SAH-SOS1$_A$–induced down-regulation of RAS-driven phosphosignaling. It is also noteworthy that pancreatic cancer cells have been shown to up-regulate macropinocytosis as a unique means of nutrient loading (28). Because appropriately designed stapled peptides can achieve cellular penetrance via the same macropinocytotic pathway, preferential uptake of therapeutic peptide by KRAS-driven pancreatic cancer cells may provide a further measure of tissue selectivity. Future directions include further optimizing the potency of prototype SAH-SOS1 peptides by using structure-activity relationships, exploring the therapeutic window for KRAS modulation in vivo by building on the *Drosophila* results, and advancing lead constructs to preclinical testing in murine models of KRAS-driven cancers.

Methods

Peptide Synthesis and Characterization. Fmoc-based automated peptide synthesis, hydrocarbon stapling by olefin metathesis, and N-terminal derivatization with FITC-β-Ala, acetyl, or Biotin-β-Ala were performed according to our established methods (22). All peptides were purified by liquid chromotography/MS to >90% purity and quantified by amino acid analysis (Table S1 and Fig. S2).

KRAS Protein Purification. Recombinant wild-type human KRAS protein (amino acids1–156) and its G12D, G12V, G12S, G12C, and Q61H mutant variants were expressed in *Escherichia coli* BL21(DE3) as N-terminal hexahistidine-tagged (His_6) fusion proteins by using the pET28-MHL expression vector (Addgene plasmid 25153; a gift from C. Arrowsmith, University of Toronto, Toronto). Protein expression was induced with 1 mM IPTG for 4 h at 30 °C. Bacterial pellets were resuspended in lysis buffer (20 mM Tris, 250 mM NaCl, pH 7.6), lysed by microfluidization (Microfluidics M-110L), and centrifuged at 45,000 rpm for 1 h at 4 °C (Beckman L-90K). The cleared cellular lysates were subjected to Ni affinity resin (Qiagen) chromatography followed by elution with 150 mM imidazole in 50 mM Tris, 250 mM NaCl, pH 7.8. Concentrated eluates were subjected to size exclusion chromatography (GE Life Sciences) at 4 °C by using 50 mM Tris, 150 mM NaCl, pH 7.8 buffer conditions, and the corresponding monomeric peaks were collected. Protein concentration was determined by Bradford assay (Bio-Rad) and UV absorbance measurements, and the average value was used. His_6-tagged KRAS proteins were used in all biochemical experiments unless otherwise indicated.

Fluorescence Polarization Assay. FP assays were performed as described (18). Briefly, FITC-SAH-SOS1 peptides (15 nM) were incubated with the indicated serial dilution of KRAS wild-type or mutant protein in binding buffer (50 mM Tris, 100 mM NaCl, pH 8.0) until equilibrium was reached (30 min). Fluorescence polarization was measured using a SpectraMax M5 microplate reader (Molecular Devices). EC_{50} values were calculated by nonlinear regression analysis of dose–response curves using Prism software (GraphPad).

Nucleotide Loading. Nucleotide loading for FP, differential scanning fluorimetry (DSF), and NMR spectroscopy studies were performed as described (21). Purified KRAS protein (200 μM) was incubated with 2 mM GDP or GppNp in loading buffer [20 mM Tris·HCl (pH 7.5), 150 mM NaCl, 5 mM EDTA, 1 mM DTT] for 1.5 h on ice. Reactions were quenched with 12 mM $MgCl_2$ and incubated for 30 min on ice. For DSF (*SI Methods*), the protein was used without further purification, whereas for NMR and FP, excess of the free nucleotides was removed and the buffer exchanged into PBS, 1 mM DTT, 2 mM $MgCl_2$ using preequilibrated NAP-5 columns (GE Life Sciences).

NMR Spectroscopy. All spectra were collected by using an Agilent Inova 500 MHz system equipped with a triple resonance (H, C, N) 5-mm cold probe. Experiments were performed at 25 °C. KRAS was uniformly ^{15}N isotopically labeled, charged with GDP as described above, and dissolved in phosphate buffer (95:5 H_2O:D_2O, PBS pH 7.4, 1.0 mM DTT, 2 mM $MgCl_2$). The instrument was locked to the deuterium signal, and resonances are reported in parts per million relative to D_2O ($\delta_H = 4.72$ ppm). A 5-mm NMR tube was charged with 500 μL of sample (100 μM protein) and the ^{15}N-heteronuclear single quantum correlation (HSQC) spectrum was recorded. Resonances were compared with the literature values (29). For titration experiments, up to 10 molar equivalents of SAH-SOS1$_A$ (in PBS) were added to the protein solution. Data were analyzed by using VNMRJ 3.2 software (Agilent Technologies). The change in chemical shift upon addition of ligand was plotted for each KRAS residue. The chemical shifts of ^1H and ^{15}N were averaged by using the formula: $Shift = \sqrt{0.5 \times [\delta_H^2 + (\alpha \times \delta_N^2)]}$, with the scale factor α taken to be 0.14 (30). The absence of a bar indicates no chemical shift change, the presence of a proline, or a residue that is overlapped or not assigned.

Docking Calculations. The peptide sequence FFGIXLTNXLKTEEGN was built by using Maestro in an idealized α-helical form. The sequence was docked to the target protein by using the HADDOCK webserver default parameters (31, 32). Chain R of the 1NVU crystal structure (21) was used, with residues L6, G15, H27, F28, V29, L56, D57, E63, Y64, R73, T74, G77, and R149 defined as the active residues. Top-scoring clusters were analyzed visually with Pymol (Schrödinger, LLC).

Nucleotide Association Assay. The association of mant-GTP with wild-type KRAS protein was monitored by fluorescence measurement over time on a Tecan X1000 fluorescence spectrometer (excitation 360 nm, emission 440 nm) (12). SAH-SOS1 peptides at the indicated amounts were incubated with 1 μM KRAS and 1 μM mant-GTP in buffer containing 25 mM Tris (pH 7.5), 50 mM NaCl, and 1 mM DTT at 25 °C. KRAS and mant-GTP alone established the positive control for association, and competition with 200-fold excess unlabeled GTP served as the negative control. The identical association experiment was performed with KRAS G12D except that mant-GDP was used instead, because

mant-GTP association was not detectable within the analogous experimental time frame.

Cell Viability Experiments. The indicated cell lines (American Type Culture Collection) were plated in 96-well plates at 10^4 cells per well by using high-glucose DMEM media supplemented with 10% (vol/vol) FBS, 1% penicillin/streptomycin and L-Glutamine (Invitrogen). The media was aspirated and SAH-SOS1 peptides were added at the indicated concentrations in serum-free DMEM. After 4 h of peptide exposure, serum was replaced [10% (vol/vol) FBS final concentration], and cell viability was measured at 24 h by CellTiterGlo assay (Invitrogen).

Phosphosignaling Western Blot Analysis. The indicated cells were plated in 12-well plates at 10^5 cells per well containing high-glucose DMEM media supplemented with 10% (vol/vol) FBS, 1% penicillin/streptomycin, and L-Glutamine. After 24 h, cells were treated with the indicated amounts of SAH-SOS1 peptides for 4 h in serum-free DMEM, followed by addition of endothelial EGF (Cell Signaling) at 10 ng/mL for 15 min. Cells were lysed in buffer containing 0.5% Nonidet P-40, 50 mM Tris (pH 7.4), 150 mM NaCl, 5 mM $MgCl_2$, Complete protease inhibitors and PhosphoOne phosphatase inhibitors (Roche), and the lysates were subjected to SDS/PAGE and Western blot analysis using antibodies to actin (Sigma) and phospho- and total Erk1/2, S6K, and MEK1/2 (Cell Signaling).

In Vivo Phosphosignaling Analysis. The *Drosophila ActinGS-Gal4* line was a gift from J. Tower, University of Southern California, Los Angeles, and the *UAS-Ras85D^{V12}* line was obtained from the Bloomington Stock Center. Flies were reared and experiments were conducted at 25 °C on a 12h:12h light-dark cycle at constant humidity by using standard sugar yeast medium, unless noted otherwise. Flies were reared on food (2 mL) containing vehicle (ethanol) or RU486 (at 150 μg/mL concentration; Cayman Chemicals) for 3 d to induce RAS expression. Pulled glass capillaries were filled with vehicle (DMSO) or SAH-SOS1 stock solution (10 mM) and flies were injected with 0.2 μL of fluid under stable pressure ($n = 5$ per treatment condition). After 48 h, flies were snap frozen in liquid nitrogen and then grinded three times for 5 min at 4 °C in buffer containing 1% Nonidet P-40, 50 mM Tris pH 7.4, 150 mM NaCl, 5 mM $MgCl_2$, and protease and phosphatase inhibitors, using a BeadBeater charged with 0.5-mm zirconium beads. Lysates were cleared by centrifugation, and the supernatants were analyzed by SDS/PAGE and Western blotting. For the peptide feeding experiments, flies ($n = 20$ per treatment condition) were placed in vials with 2 mL of food containing vehicle (ethanol), RU486 alone (150 μg/mL), or the combination of RU486 with 20 μL of vehicle (DMSO) or 20 μL of SAH-SOS1$_A$ or SAH-SOS1$_B$ stock solutions to achieve final peptide concentrations of 1, 10, or 100 μM. Flies were collected after 4 d, processed, and lysates were analyzed as described above. For the time-course experiments, flies were reared on 2 mL of chemically defined food (Harlan) containing vehicle, RU486 alone (150 μg/mL), or the combination of RU486 with 20 μL of vehicle (DMSO) or 20 μL of 10 mM stock solutions of SAH-SOS1$_A$ or SAH-SOS1$_B$ peptides (final peptide concentration of 100 μM). After 3 or 5 d, the flies were collected, processed, and lysates analyzed as above. Antibodies for Western blot analysis included tubulin (Sigma), phospho- and total ERK1/2 (Cell Signaling), and RAS (gift of M. Therrien, University of Montreal, Montreal).

ACKNOWLEDGMENTS. We thank Eric D. Smith for figure preparation and graphics assistance, Marc Therrien for Ras1 antibodies, and John Tower for Actin-GS-Gal4 flies. This work was supported by NIH Grant 5R01GM090299 (to L.D.W.), NIH Grant P01CA120964 and Howard Hughes Medical Institute (to N.P.), an American Association of University Women International Fellowship (to E.S.L.), NIH Grant T32GM007753 (to J.L.), the Todd J. Schwartz Memorial Fund, and the Wolpoff Family Foundation.

1. Karnoub AE, Weinberg RA (2008) Ras oncogenes: Split personalities. *Nat Rev Mol Cell Biol* 9(7):517–531.
2. Stephen AG, Esposito D, Bagni RK, McCormick F (2014) Dragging ras back in the ring. *Cancer Cell* 25(3):272–281.
3. Hidalgo M (2010) Pancreatic cancer. *N Engl J Med* 362(17):1605–1617.
4. Lim SM, et al. (2014) Therapeutic targeting of oncogenic K-Ras by a covalent catalytic site inhibitor. *Angew Chem Int Ed Engl* 53(1):199–204.
5. Ostrem JM, Peters U, Sos ML, Wells JA, Shokat KM (2013) K-Ras(G12C) inhibitors allosterically control GTP affinity and effector interactions. *Nature* 503(7477):548–551.
6. Shima F, et al. (2013) In silico discovery of small-molecule Ras inhibitors that display antitumor activity by blocking the Ras-effector interaction. *Proc Natl Acad Sci USA* 110(20):8182–8187.
7. Chardin P, et al. (1993) Human Sos1: A guanine nucleotide exchange factor for Ras that binds to GRB2. *Science* 260(5112):1338–1343.
8. Olivier JP, et al. (1993) A Drosophila SH2-SH3 adaptor protein implicated in coupling the sevenless tyrosine kinase to an activator of Ras guanine nucleotide exchange, Sos. *Cell* 73(1):179–191.
9. Konstantinopoulos PA, Karamouzis MV, Papavassiliou AG (2007) Post-translational modifications and regulation of the RAS superfamily of GTPases as anticancer targets. *Nat Rev Drug Discov* 6(7):541–555.
10. Patgiri A, Yadav KK, Arora PS, Bar-Sagi D (2011) An orthosteric inhibitor of the Ras-Sos interaction. *Nat Chem Biol* 7(9):585–587.
11. Maurer T, et al. (2012) Small-molecule ligands bind to a distinct pocket in Ras and inhibit SOS-mediated nucleotide exchange activity. *Proc Natl Acad Sci USA* 109(14):5299–5304.
12. Sun Q, et al. (2012) Discovery of small molecules that bind to K-Ras and inhibit Sos-mediated activation. *Angew Chem Int Ed Engl* 51(25):6140–6143.
13. Burns MC, et al. (2014) Approach for targeting Ras with small molecules that activate SOS-mediated nucleotide exchange. *Proc Natl Acad Sci USA* 111(9):3401–3406.
14. Wu X, et al. (2013) Inhibition of Ras-effector interaction by cyclic peptides. *Med Chem Comm* 4(2):378–382.
15. Bernal F, et al. (2010) A stapled p53 helix overcomes HDMX-mediated suppression of p53. *Cancer Cell* 18(5):411–422.
16. Kim W, et al. (2013) Targeted disruption of the EZH2-EED complex inhibits EZH2-dependent cancer. *Nat Chem Biol* 9(10):643–650.
17. Takada K, et al. (2012) Targeted disruption of the BCL9/beta-catenin complex inhibits oncogenic Wnt signaling. *Sci Transl Med* 4(148):148ra117.
18. Walensky LD, et al. (2004) Activation of apoptosis in vivo by a hydrocarbon-stapled BH3 helix. *Science* 305(5689):1466–1470.
19. Chang YS, et al. (2013) Stapled α-helical peptide drug development: A potent dual inhibitor of MDM2 and MDMX for p53-dependent cancer therapy. *Proc Natl Acad Sci USA* 110(36):E3445–E3454.
20. Bird GH, et al. (2014) Mucosal delivery of a double-stapled RSV peptide prevents nasopulmonary infection. *J Clin Invest* 124(5):2113–2124.
21. Margarit SM, et al. (2003) Structural evidence for feedback activation by Ras.GTP of the Ras-specific nucleotide exchange factor SOS. *Cell* 112(5):685–695.
22. Bird GH, Crannell WC, Walensky LD (2011) Chemical synthesis of hydrocarbon-stapled peptides for protein interaction research and therapeutic targeting. *Curr Protoc Chem Biol* 3(3):99–117.
23. Walensky LD, Bird GH (2014) Hydrocarbon-stapled peptides: Principles, practice, and progress. *J Med Chem* 57(15):6275–6288.
24. Milburn MV, et al. (1990) Molecular switch for signal transduction: Structural differences between active and inactive forms of protooncogenic ras proteins. *Science* 247(4945):939–945.
25. Zhang J, Matthews CR (1998) Ligand binding is the principal determinant of stability for the p21(H)-ras protein. *Biochemistry* 37(42):14881–14890.
26. Karim FD, Rubin GM (1998) Ectopic expression of activated Ras1 induces hyperplastic growth and increased cell death in Drosophila imaginal tissues. *Development* 125(1):1–9.
27. Ford D, et al. (2007) Alteration of Drosophila life span using conditional, tissue-specific expression of transgenes triggered by doxycyline or RU486/Mifepristone. *Exp Gerontol* 42(6):483–497.
28. Commisso C, et al. (2013) Macropinocytosis of protein is an amino acid supply route in Ras-transformed cells. *Nature* 497(7451):633–637.
29. Vo U, Embrey KJ, Breeze AL, Golovanov AP (2013) ^{1}H, ^{13}C and ^{15}N resonance assignment for the human K-Ras at physiological pH. *Biomol NMR Assign* 7(2):215–219.
30. Williamson MP (2013) Using chemical shift perturbation to characterise ligand binding. *Prog Nucl Magn Reson Spectrosc* 73:1–16.
31. de Vries SJ, van Dijk M, Bonvin AMJJ (2010) The HADDOCK web server for data-driven biomolecular docking. *Nat Protoc* 5(5):883–897.
32. Wassenaar TA, et al. (2012) WeNMR: Structural biology on the grid. *J Grid Comput* 10(4):743–767.

Supporting Information

Leshchiner et al. 10.1073/pnas.1413185112

SI Methods

Fluorescence Size Exclusion Chromatography. FSEC was performed on an Agilent 1260 HPLC equipped with a fluorescence detector. A 100-μL solution of 0.5 μM or 10-μL solution of 10 μM FITC-SAH-SOS1$_A$ was injected onto a 10/100 GL Superdex 75 gel permeation column and eluted in 50 mM Tris(hydroxymethyl) aminomethane hydrochloride (pH 8) containing 150 mM NaCl, using a flow rate of 0.5 mL/min.

Differential Scanning Fluorimetry. Differential scanning fluorimetry (DSF), or thermal shift, assay was performed on a Roche LightCycler 480 II with ramp speed of 4.8 °C per min and 12 acquisitions per °C. Solutions of KRAS/SAH-SOS1 peptide (10 μM) with added SYPRO dye (Life Technologies; 1:1,000 dilution) was dispensed into 384-well polypropylene PCR plates (10 μL per well). The plates were sealed and heated in the instrument across a temperature range of 25–95 °C.

SOS1/KRAS Dissociation Assay. The catalytic domain of SOS1 protein (amino acids 564–1049) was cloned into the pET-28a vector and produced in *E. coli* BL21(DE3) as a His$_6$-tagged fusion protein. Protein expression was induced by 1 mM IPTG at 30 °C for 4 h, and His$_6$-SOS1 was purified using Ni-NTA affinity resin (Qiagen) and eluted with 150 mM imidazole in 50 mM Tris, 150 mM NaCl, pH 7.8, followed by size exclusion chromatography (GE Life Sciences) in 50 mM Tris, 150 mM NaCl, pH 7.8 buffer conditions. GST-KRAS (amino acids 1–188; Abnova) was subjected to buffer exchange (50 mM Tris, 150 mM NaCl, pH 7.8) using Amicon filter units (3 kDa molecular mass cutoff; Millipore). For in vitro immunoprecipitation studies, an equimolar mixture of recombinant GST-KRAS and His$_6$-SOS1 catalytic domain (amino acids 564–1049) (1 μM each, 300 μL of reaction volume) was incubated with vehicle, SAH-SOS1$_A$, or SAH-SOS1$_B$ peptides (5, 10 μM) at 25 °C for 40 min. The experimental solutions were transferred to preblocked [3% (wt/vol) BSA in PBS] glutathione resin beads (GE Healthcare Life Sciences) and incubated at 4 °C with constant mixing for 1 h, followed by three washes with 1% BSA in PBS, and resuspension of beads in LDS for SDS/PAGE and anti-KRAS (Cell Signaling) and anti-His$_6$ (Abcam) Western blot analysis.

KRAS Pull-Down Assay. Biotin-labeled SAH-SOS1$_A$ (10 μM) or vehicle (0.2% DMSO) was incubated with streptavidin-Sepharose in PBS at 4 °C for 1 h. The beads were then blocked with 2 mg/mL biotin (40 min) and 3% (wt/vol) BSA (40 min), and recombinant His$_6$-KRAS was added to the beads at a final concentration of 10 μM in 1% (wt/vol) BSA. The beads were then rotated at 4 °C for 1 h, washed three times with 1% BSA in PBS, and resuspended in LDS for SDS/PAGE and anti-KRAS (Cell Signaling) Western blot analysis.

Cellular Uptake Analysis. Panc 10.05 cells were plated at 4×10^5 cells per well in 35-mm poly-D-lysine–coated dishes (MatTek). The cells were treated with 0.5 μM FITC-SAH-SOS1 peptides for 2 h in serum-free DMEM and then stained with Hoechst dye and CellMask Orange (Invitrogen) for 10 min. The media was aspirated and the cells fixed with 4% (wt/vol) paraformaldehyde for 10 min at 4 °C, washed three times with PBS, and imaged using a Yokogawa CSU-X1 spinning disk confocal system (Andor Technology) attached to a Nikon Ti-E inverted microscope (Nikon Instruments; excitation with 405-, 488-, and 561-nm lasers). Images were acquired using a 100× Plan Apo objective lens with a Hamamatsu OrcaER camera (Hamamatsu Photonics). The data were analyzed by ImageJ software. At least six fields of view were collected for each experimental condition. As a second measure of peptide uptake, Panc 10.05 cells were plated in 12-well plates at 4×10^5 cells per well and then treated as above with the indicated doses of SAH-SOS1 peptides for 2 h, followed by aspiration of the media, PBS washes, and trypsinization. Cells were collected, washed three times with PBS, and lysed in buffer containing 1% (vol/vol) Nonidet P-40, 50 mM Tris, 150 mM NaCl, pH 7.4, supplemented with protease and phosphatase inhibitor tablets (Roche). The lysates were electrophoresed on 4–12% Bis-Tris gels (Invitrogen), which were then subjected to fluorescence imaging using a Typhoon 9400 (GE Healthcare).

High-content fluorescence microscopy analysis to evaluate intracellular FITC peptide was performed as described (1). The indicated cell lines were plated in black, clear bottom plates overnight at a density of 2×10^4 cells per well in DMEM supplemented with 10% (vol/vol) FBS, 1% penicillin/streptomycin, and 1% glutamine. The following day, cells were treated with 0.5 μM FITC-labeled SAH-SOS1 peptides or the equivalent amount of vehicle (0.1% DMSO) or FITC for 4 h in serum-free DMEM, and then stained with Hoechst dye and CellMask Deep Red (CMDR, Invitrogen) for 10 min. The media was aspirated, and cells were fixed with 4% (wt/vol) paraformaldehyde for 10 min, washed three times with PBS and imaged by ImageXpress Microscopy (high-throughput epifluorescence microscope; Molecular Devices). Data were collected for five sites per well, with each treatment performed in duplicate, and then analyzed and quantified using MetaXpress software. The CMDR stain was used to visualize the boundaries of the cell and to create a mask for measuring FITC-peptide inside the cell, thereby excluding fluorescent debris from the analysis. A custom module in MetaXpress was applied to incrementally recede the CMDR image mask from the cellular border, further restricting the analyzed FITC signal to internalized peptide. In addition, only FITC signal that exceeded an intensity threshold of 10 times above local background was incorporated into the analysis.

1. Moellering RE, et al. (2009) Direct inhibition of the NOTCH transcription factor complex. *Nature* 462(7270):182–188.

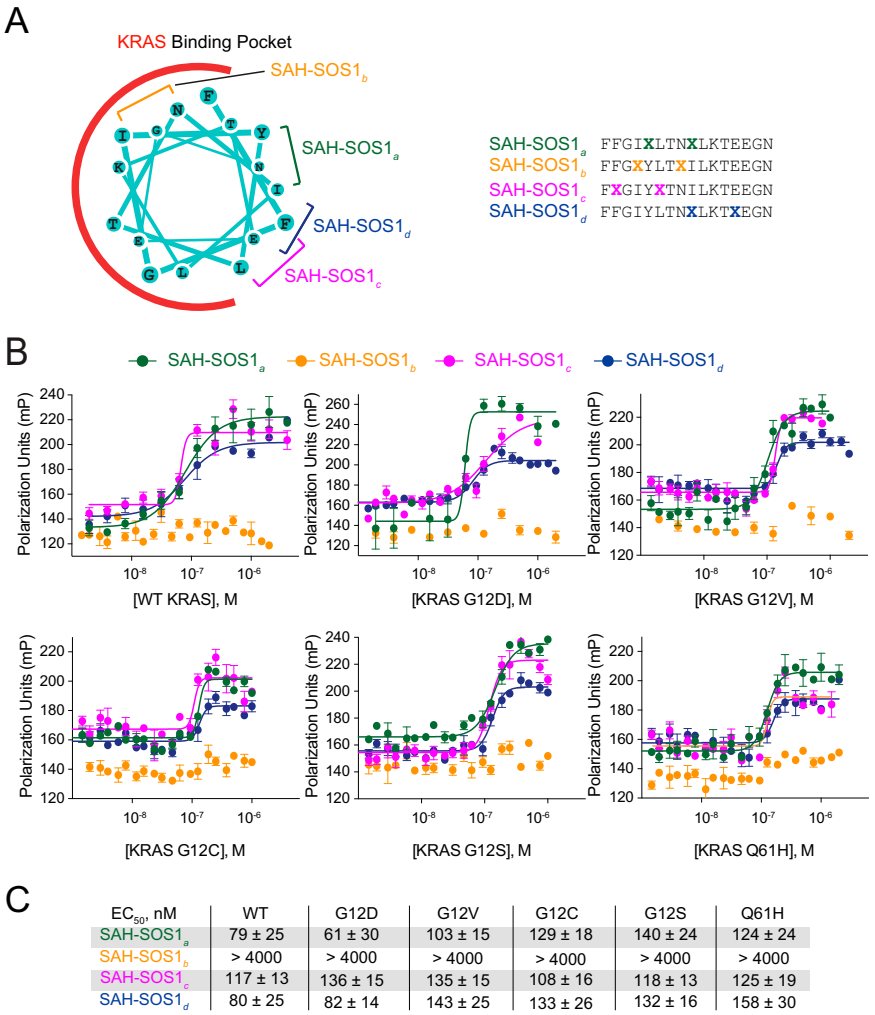

C

EC_{50}, nM	WT	G12D	G12V	G12C	G12S	Q61H
SAH-SOS1$_a$	79 ± 25	61 ± 30	103 ± 15	129 ± 18	140 ± 24	124 ± 24
SAH-SOS1$_b$	> 4000	> 4000	> 4000	> 4000	> 4000	> 4000
SAH-SOS1$_c$	117 ± 13	136 ± 15	135 ± 15	108 ± 16	118 ± 13	125 ± 19
SAH-SOS1$_d$	80 ± 25	82 ± 14	143 ± 25	133 ± 26	132 ± 16	158 ± 30

Fig. S1. Design and KRAS binding activity of SAH-SOS1 peptides. (*A*) SAH-SOS1 peptides for KRAS targeting were generated by inserting all-hydrocarbon staples at positions a (green), b (orange), c (pink), and d (blue) into a SOS1 peptide spanning amino acids 929–944. (*B*) Fluorescence polarization binding analysis of FITC-labeled SAH-SOS1 peptides and recombinant KRAS proteins, including wild-type and mutant variants. Data are mean ± SEM for experiments performed in technical triplicate and are representative of at least three biological replicates performed with independent preparations of recombinant KRAS proteins. (*C*) Table of EC_{50} values for the binding interactions between SAH-SOS1 peptides and the individual KRAS proteins.

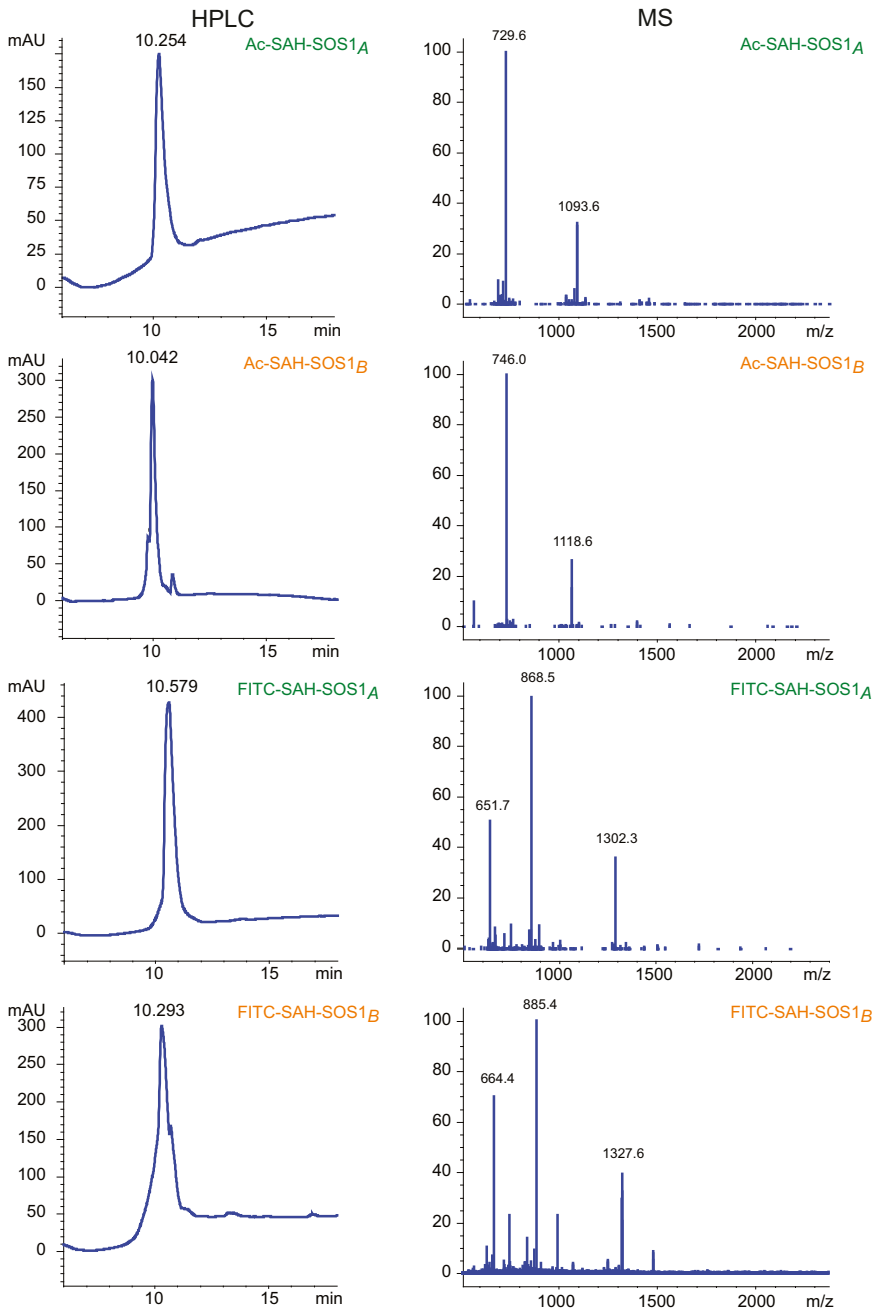

Fig. S2. Purification and mass spectrometry analysis of SAH-SOS1 peptides. HPLC (*Left*) and MS profiles (*Right*) of Ac-SAH-SOS1$_A$, Ac-SAH-SOS1$_B$, FITC-SAH-SOS1$_A$, and FITC-SAH-SOS1$_B$ peptides document compound purity (>90%) and mass identify, respectively.

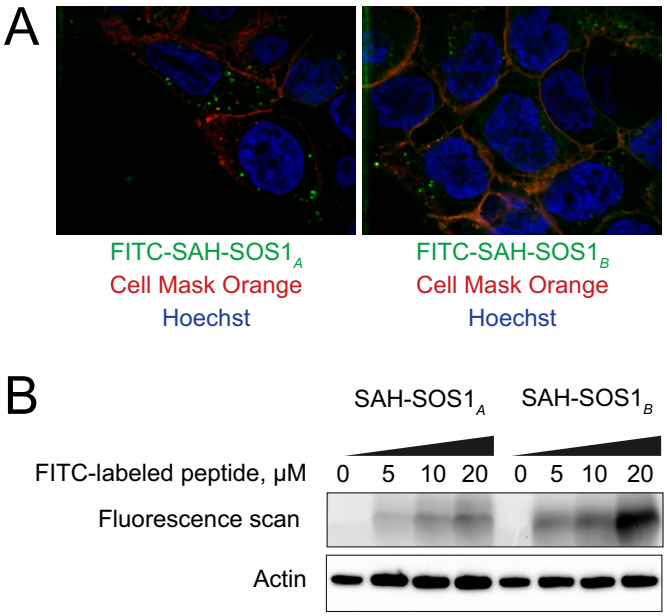

Fig. S3. Cellular uptake of SAH-SOS1$_A$ and SAH-SOS1$_B$ peptides. (*A*) FITC-derivatized analogs of SAH-SOS1$_A$ and SAH-SOS1$_B$ peptides bearing N-terminal Arg-Arg residues were applied to cultured Panc 10.05 cells, and cellular fluorescence was examined by confocal microscopy. Cell Mask Orange (plasma membrane), red; FITC, green; Hoechst (nucleus), blue. At least six fields of view were acquired per experimental condition; the data are representative of two biological replicates performed with independent cancer cell cultures. (*B*) FITC-SAH-SOS1 peptide uptake was also monitored by fluorescence scan of electrophoresed lysates from treated Panc 10.05 cells. Data are representative of at least three biological replicates performed with independent cancer cell cultures.

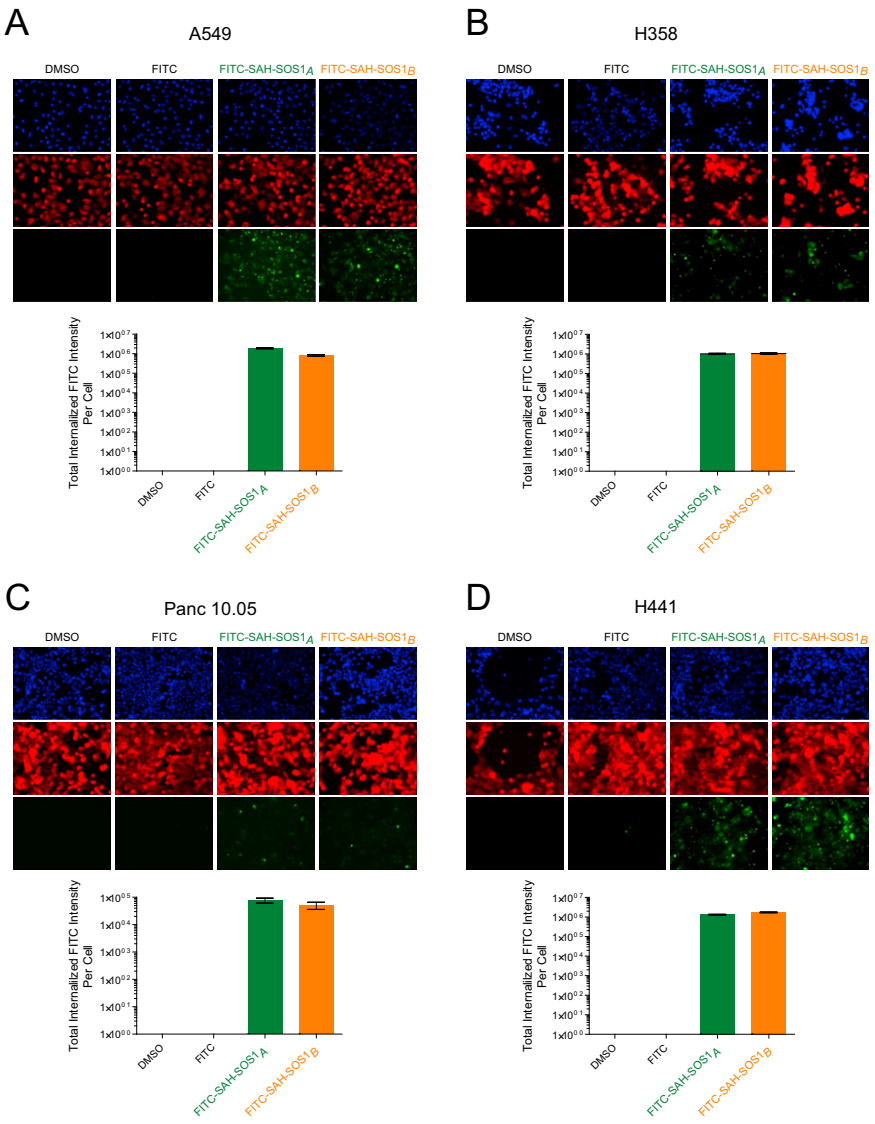

Fig. S4. High content microscopic imaging analysis of SAH-SOS1 peptide uptake by KRAS-driven cancer cell lines. High throughput epifluorescence microscopy and image analysis (MetaXpress) demonstrate fluorescence of A549 (*A*), H358 (*B*), Panc 10.05 (*C*), and H441 (*D*) cells treated with FITC-SAH-SOS1$_A$ or FITC-SAH-SOS1$_B$ peptides (0.5 μM), but not the vehicle (0.1% DMSO) or FITC-only controls. The nuclear (Hoechst 33342, blue) and plasma membrane (CellMask Deep Red, red) channels were used to create a mask, such that green intensity located inside the cellular boundary was measured on a per cell basis over five fields, averaged, and then plotted. Data are mean ± SEM for experiments performed in technical duplicate and then repeated with independent cancer cell cultures and treatment.

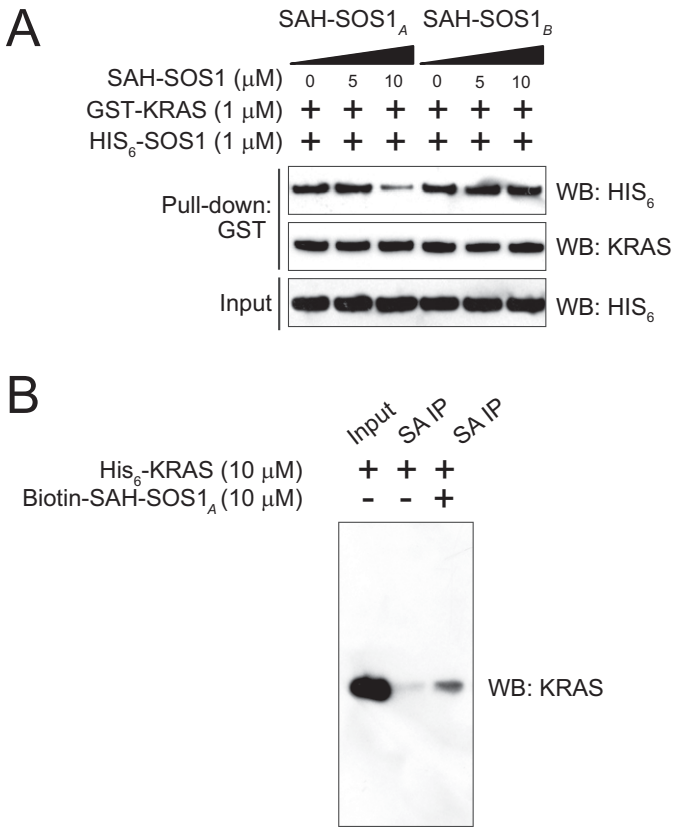

Fig. S5. Dissociation of the SOS1/KRAS protein interaction by SAH-SOS1$_A$. (*A*) SAH-SOS1$_A$, but not SAH-SOS1$_B$, disrupts the protein interaction between GST-KRAS (1 μM) and His$_6$-SOS1 (1 μM), as evidenced by GST pull-down and anti-KRAS and anti-His$_6$ Western blot analysis. (*B*) SAH-SOS1$_A$ directly targets recombinant KRAS in solution, as evidenced by streptavidin pull-down of the Biotin-SAH-SOS1$_A$/KRAS complex.

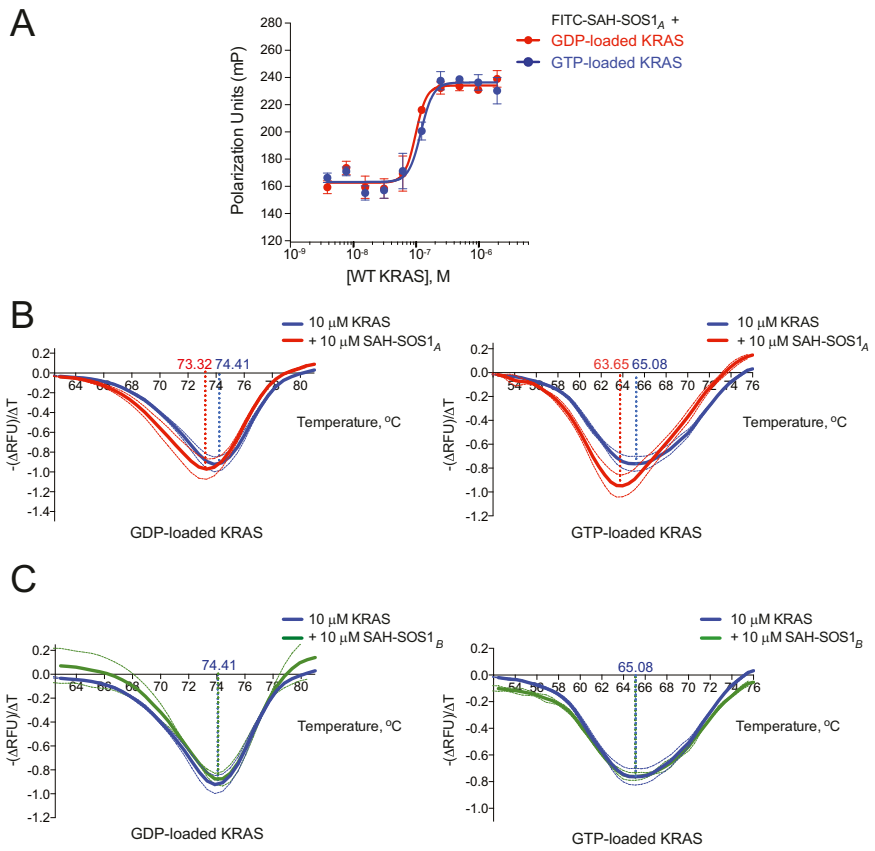

Fig. S6. SAH-SOS1$_A$ binds to GDP- and GTP-loaded forms of KRAS. (*A*) Fluorescence polarization binding analysis of FITC-SAH-SOS1$_A$ and recombinant wild-type KRAS protein, loaded with GDP (red) or GTP (blue). Data are mean ± SD for experiments performed in technical triplicate and representative of at least two biological replicates performed with independent preparations of recombinant KRAS proteins. (*B* and *C*) Differential scanning fluorimetry was performed on GDP- or GTP-loaded forms of recombinant wild-type KRAS (blue), in the presence or absence of SAH-SOS1$_A$ (red) (*B*) or the negative control SAH-SOS1$_B$ peptide (green) (*C*). Data are mean ± SD (dotted lines) for experiments performed in triplicate and representative of three biological replicates using independent KRAS preparations.

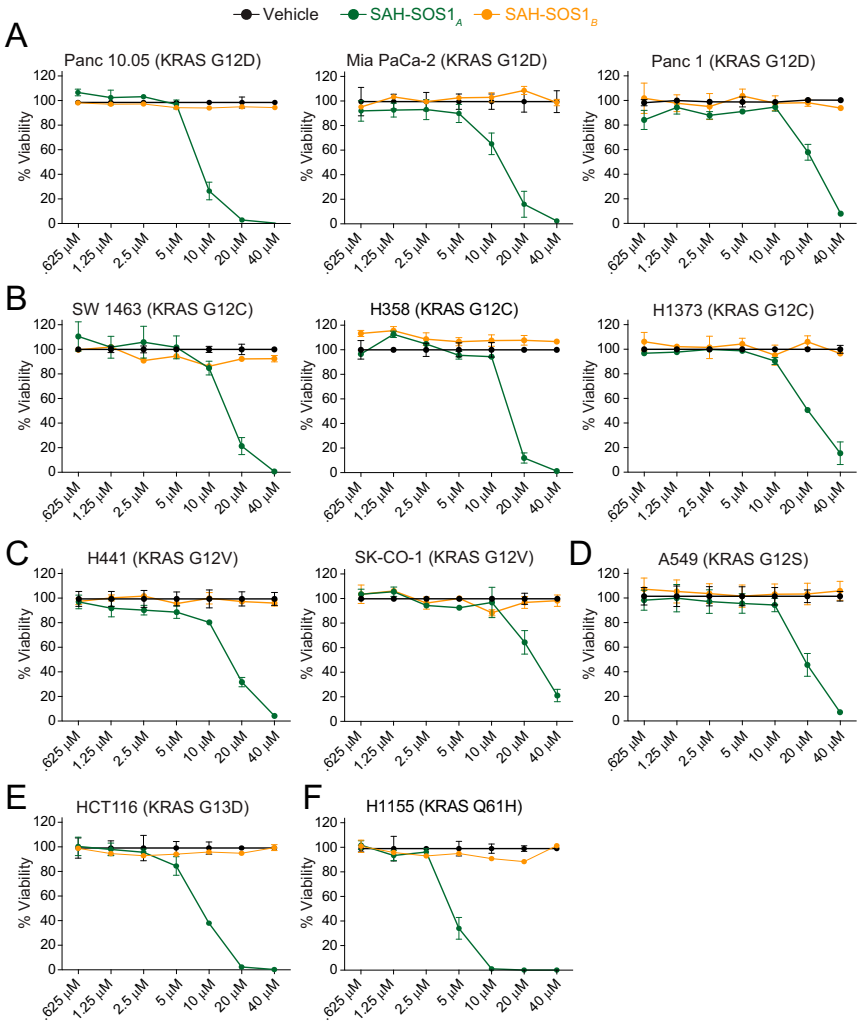

Fig. S7. SAH-SOS1$_A$ inhibits the viability of mutant KRAS-expressing cancer cells in a dose- and sequence-dependent manner. Cancer cells bearing KRAS G12D (*A*), KRAS G12C (*B*), KRAS G12V (*C*), KRAS G12S (*D*), KRAS G13D (*E*), and KRAS Q61H (*F*) were treated with vehicle, SAH-SOS1$_A$, or SAH-SOS1$_B$, and cell viability was measured at 24 h by CellTiterGlo assay. Data are mean ± SEM for experiments performed in at least duplicate and representative of at least two biological replicates performed with independent cancer cell cultures.

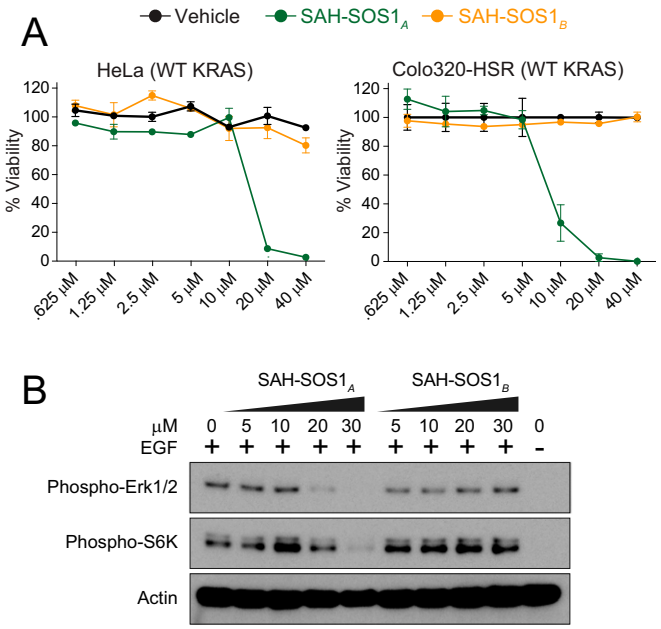

Fig. S8. SAH-SOS1$_A$ cytotoxicity correlates with inhibition of phosphosignaling downstream of KRAS. (*A*) HeLa and Colo320-HSR cells bearing wild-type KRAS were treated with vehicle, SAH-SOS1$_A$, or SAH-SOS1$_B$ peptides and cell viability measured at 24 h by CellTiterGlo assay. Data are mean ± SEM for experiments performed in at least technical duplicates and representative of at least two biological replicates performed with independent cancer cell cultures. (*B*) Panc 10.05 cells were incubated with vehicle, SAH-SOS1$_A$, or SAH-SOS1$_B$ at the indicated doses for 4 h, followed by 15 min of stimulation with EGF. Cellular lysates were then electrophoresed and subjected to Western blot analysis using antibodies to phospho- and total MEK1/2, ERK1/2, and Akt.

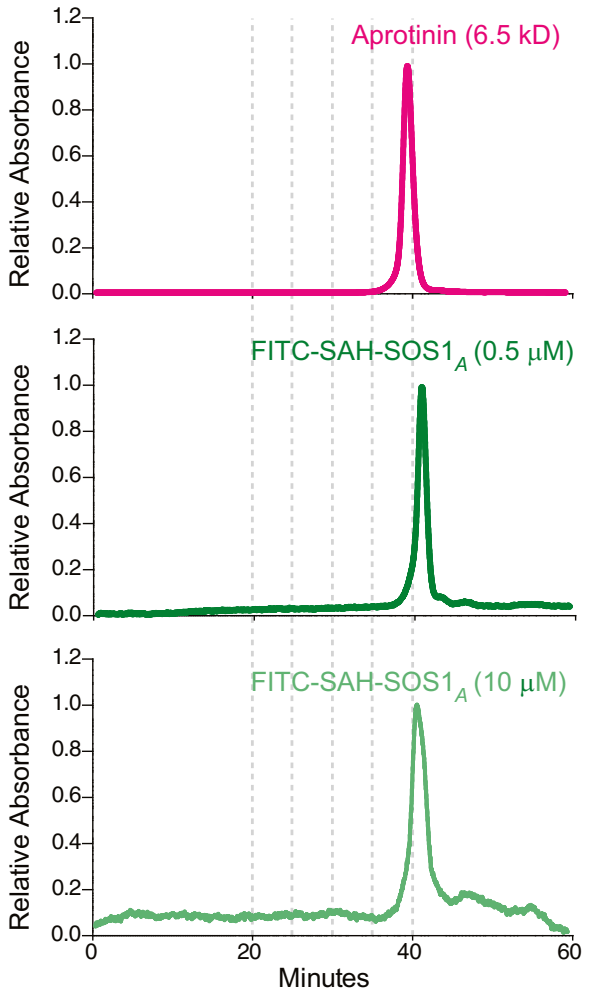

Fig. S9. Fluorescence size exclusion chromatography (FSEC) of SAH-SOS1$_A$ solutions. FSEC analysis of 0.5 μM and 10 μM solutions of FITC-SAH-SOS1$_A$ peptide demonstrate a monodispersed peak, reflecting a monomeric species eluting at ~3 kDa with respect to the aprotinin molecular mass standard (6.5 kDa).

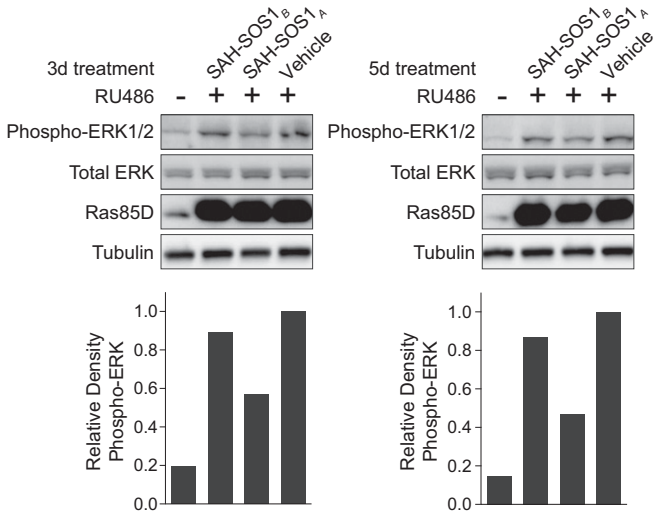

Fig. S10. SAH-SOS1$_A$ inhibits phosphosignaling downstream of KRAS in a *D. melanogaster* model of RAS activation. *D. melanogaster* Ras85D^{V12}/ActinGS (n = 20 per treatment arm) were exposed to chemically defined medium supplemented with vehicle or RU486 (150 μg/mL) for 2 d. RAS-induced flies were then treated with vehicle (DMSO), SAH-SOS1$_A$, or SAH-SOS1$_B$, added to a final concentration of 100 μM in 2 mL of fresh food containing RU486 (150 μg/mL). After 3 or 5 d of oral peptide treatment, the flies were collected and tissue lysates subjected to electrophoresis and Western blotting using RAS, and phospho- and total ERK1/2 antibodies. Western bands were quantified with ImageJ software.

Table S1. SAH-SOS1 peptide compositions

Peptide	Sequence	N terminus	MW	M+3/3	Fig.
SAH-SOS1$_a$	FFGIXLTNXLKTEEGN	FITC-βAla	2,292	765	S1
SAH-SOS1$_b$	FFGXYLTXILKTEEGN	FITC-βAla	2,341	781	S1
SAH-SOS1$_c$	FXGIYXTNILKTEEGN	FITC-βAla	2,308	770	S1
SAH-SOS1$_d$	FFGIYLTNXLKTXEGN	FITC-βAla	2,326	776	S1
SAH-SOS1$_A$	RRFFGIXLTNXLKTEEGN	FITC-βAla	2,604	869	1, S2–S4, S9
SAH-SOS1$_A$	RRFFGIXLTNXLKTEEGN	Ac	2,186	730	2–5, S2, S5–S8, S10
SAH-SOS1$_A$	RRFFGIXLTNXLKTEEGN	Biotin-βAla	2,441	815	S5
SAH-SOS1$_B$	RRFFGXYLTXILKTEEGN	FITC-βAla	2,654	886	1, S2–S4
SAH-SOS1$_B$	RRFFGXYLTXILKTEEGN	Ac	2,236	746	3–5,S2,S5–S8, S10
SAH-SOS1$_A$mut1	RRFFGKXLTNXLKTEEGN	FITC-βAla	2,619	874	4
SAH-SOS1$_A$mut1	RRFFGKXLTNXLKTEEGN	Ac	2,201	735	4
SAH-SOS1$_A$mut2	RRFFGIXLTRXLKTEEGN	FITC-βAla	2,647	883	4
SAH-SOS1$_A$mut2	RRFFGIXLTRXLKTEEGN	Ac	2,229	744	4
SAH-SOS1$_A$mut3	RRFFGIXDTNXLKTEEGN	FITC-βAla	2,606	870	4
SAH-SOS1$_A$mut3	RRFFGIXDTNXLKTEEGN	Ac	2,188	730	4
SAH-SOS1$_A$mut4	RRFFGIXKTNXLKTEEGN	FITC-βAla	2,619	874	4
SAH-SOS1$_A$mut4	RRFFGIXKTNXLKTEEGN	Ac	2,201	735	4
SAH-SOS1$_A$mut5	RRFEGIXRLEXLKAEEAN	FITC-βAla	2,640	881	4
SAH-SOS1$_A$mut5	RRFEGIXRLEXLKAEEAN	Ac	2,222	742	4